Journal of Solid State Electrochemistry (2021) 25:535–544
https://doi.org/10.1007/s10008-020-04827-4

ORIGINAL PAPER

Preparation of graphene oxide/poly(o-phenylenediamine) hybrid composite via facile in situ assembly and post-polymerization technology for the anode material of lithium ion battery

Chang Su[1] · Jiaojiao Ma[1] · Bing Han[1] · Lihuan Xu[1]

Received: 2 June 2020 / Revised: 15 September 2020 / Accepted: 18 September 2020 / Published online: 29 September 2020

Abstract

Electrode material is a key factor for high-energy storage battery. In this paper, graphene oxide/poly(o-phenylenediamine) (GO/PoPD) hybrid composite is prepared by combining the self-assembly process to form graphene oxide/o-phenylenediamine hydrogel and subsequently the in situ oxidation polymerization, which exhibits the open porous morphology with high BET surface area of 347 m^2/g. As the anode of lithium ion battery, GO/PoPD possesses the double lithium storage mechanisms from graphene oxide and poly(o-phenylenediamine). Meanwhile, it exhibits an initial discharge-specific capacity of 1632.4 mAh/g and the improved cycling stability. Even after 43 cycles, it still keeps a capacity of 839.5 mAh/g, which is obviously higher than that of GO and PoPD. Furthermore, GO/PoPD hybrid composite presents the enhanced rate performances with the discharge-specific capacities of 1411.7, 718.2, 621.2, and 576.3 mAh/g at current rates of 50, 100, 200, and 500 mA/g, respectively. The improved electrochemical performances are attributed to the formed stable porous morphology, which facilitates the electrolyte ion to penetrate into the electrode matrix during the redox reaction and then results in the improved cell performances.

Keywords Poly(phenylenediamine) derivative · Graphene · Hybrid electrode · Lithium ion battery

Introduction

Lithium-ion batteries (LIBs) have been widely applied in many fields ranging from mobile phones to automobiles. Electrode material as one of the cell components is the very key factor for a high-energy storage battery, so the new electrode material is urgently required for obtaining batteries with high performances. Carbon-based materials have become a very promising candidate for the anode of battery since the commercial applications of LIBs. It possesses the low Li intercalation potential (~ 0.1 V vs Li/Li^+) [1] and the small volume change during lithium ion intercalation/deintercalation process, which results in the batteries with carbon materials as the anode having the high cell voltage, the high coulombic efficiency, and the low capacity fade. Furthermore, a stable solid-electrolyte interphase (SEI) can form on the surface of carbon anode during the initial charge/discharge cycles, which can prevent further electrolyte decomposition and then allows for its stable work in the following charge/discharge process [2]. Just now, various carbon materials have been explored as the anode, such as graphite, amorphous carbon, hard carbon, carbon black, graphene and carbon nanotubes, and so on [3–7].

Although a lot of efforts have been made [8–10], the exploration of new carbon materials with high electrochemical performances still continues. As an alternative, graphene has attracted wide attention as a promising LIBs anode, owing to its unique two-dimensional (2D), large specific surface area and high theoretical specific capacity of double graphite (744 mAh/g) [11–13]. In the conventional fabrication of graphene-based electrode materials, the direct chemical oxidation exfoliation method is frequently applied to obtain graphene oxide (GO). However, due to the high aspect ratio of GO sheets and van der Waals interactions, the exfoliated graphene sheets tend to restack to form a bulk graphite-like structure [14], leading to the serious loss of high specific surface for Li insertion and the subsequent severe decrease in specific capacity and rate capability of the electrode [12]. Therefore, it is

✉ Chang Su
suchang@syuct.edu.cn

✉ Lihuan Xu
xulihuanss@163.com

[1] College of Chemical Engineering, Shenyang University of Chemical Technology, Shenyang 110142, People's Republic of China

necessary to develop synthesis strategies for preserving the interlayer space and Li insertion sites of graphene, in which the assembling three-dimensional (3D) graphene networks with controlled micro/meso/macropore morphology is a feasible strategy [15–17, 18]. Conventional approaches for 3D porous graphene structures include the sacrificial inorganic template method [16, 19, 20], organic template-assisted method, and self-assembly strategies [17, 21]. Recently, great efforts have been focused on the preparation of porous graphene hydrogels, in which graphene hydrogel is assembled by various non-covalent interactions [22] or through the assistance with various polymers [23, 24], such as macromolecules [25], small organic molecules [22, 26], or cations [27]. And the constructed 3D porous structure can improve the stability of porous graphene gel, increase the Li ion diffusion, and provide additional Li ion storage sites [16, 19], which is greatly promising in the energy storage field, such as lithium ion batteries and super-capacitor [28, 29].

Different from polyaniline, poly(o-phenylenediamine) (PoPD) with a ladder polymer structure contains phenazine rings and is thus an electroactive polymer of the aromatic diamines family [30]. The distinctive ladder backbone structure endows PoPD with strong withstanding to over-oxidation during the charging process, and the extended π-conjugation structure in PoPD is in favor of electron migration along the polymer chain, which made it superior to polyaniline in energy storage, such as batteries and supercapacitors [31, 32]. In this work, graphene oxide/o-phenylenediamine (GO/oPD) hydrogel with the open morphology was firstly prepared with o-phenylenediamine (oPD) as organic small molecules by self-assembly method. Furthermore, the stable graphene oxide/poly(o-phenylenediamine) (GO/PoPD) hybrid composite with PoPD as the electroactive material and the spacer between graphene sheets was prepared by in situ oxidation polymerization of o-phenylenediamine among graphene oxide (GO) sheets. Just now, there are few reports on obtaining the GO and aromatic diamines contained composite by the GO-based hydrogel and post-polymerization process, in which the obtained GO/PoPD hybrid composite possesses a stable and open porous structure. Furthermore, the fabricated GO/ PoPD composite was explored as the anode of lithium ion battery, and its electrochemical and cell performances were explored in detail.

Experimental

Material and synthesis

Material Hydrochloric acid (HCl, 36–38%) was purchased from Tianjin Dongfang Chemical Factory, ammonium persulfate ($(NH_4)_2S_2O_8$, 98%) (APS) and o-phenylenediamine (98.5%) were purchased from Sinopharm Chemical Reagent Co., Ltd., and graphite powder (95–99.9%) was purchased from Qingdao Huatai Lubrication Sealing Technology Co., Ltd. All other reagents were of analytical grade and used without further purification.

Synthesis of GO and GO/PoPD composite Graphene oxide (GO) was prepared by the modified Hummers method [33], and then via ultrasonic exfoliation in an ethanol/deionized water mixing solvent environment at low temperature. For GO/PoPD composite, the construction process was described as follows: 5 mg of the obtained GO was firstly ultrasonic-dispersed in hydrous solution (10 mL), and oPD monomer (20 mg) was then added. The resulted mixture was ultrasonic-treated for 2 h to obtain GO/oPD mixture, and subsequently, the GO/oPD mixture was hydrothermal-reacted at 150 °C for 24 h to achieve black self-assembly aggregation. For the graphene oxide/poly(o-phenylenediamine) (GO/PoPD) hybrid composite, it was prepared in situ polymerization of o-phenylenediamine in GO using $(NH_4)_2S_2O_8$ (APS) as oxidant. Specifically, an oxidant solution containing 42.2 g of APS in 20 ml of 0.1 M HCl solution was added dropwise into the abovementioned GO/oPD hybrid hydrogel aggregation, and the in situ polymerization reaction was carried out statically at room temperature for 6 h. The as-prepared hybrid composite was washed repeatedly with deionized water for several times. This prepared hybrid composite was named as GO/PoPD based on its composition. For comparison, pure PoPD without GO was also prepared by the same procedure without the addition of GO.

Material characterization

FT-IR spectra were carried out on a Nicolet 6700 spectrometer (Thermo Fisher Nicolet, USA) with KBr pellets. Scanning electron microscopy (SEM) measurements were taken using a Hitachi S-4800 scanning electron microscope (Hitachi, Japan). Thermogravimetric analyses (TGA) were performed on a Q5000IR (Ra, USA) thermogravimetric analyzer running from room temperature to 800 °C at a heating rate of 10 °C/min in air. BET was carried out on a Surface Area and Porosity Analyzer (Micromeritics, ASAP2020).

Electrochemical measurements

For obtaining electrode characterization, the electrodes were prepared by coating a mixture slurry containing 50 wt% as prepared active materials, 40 wt% Super P and 10 wt% PVDF binder in N-methyl-2-pyrrolidone (NMP) on Cu collector foils, followed by drying at 70 °C for 24 h in a vacuum. And the loading mass of the composite on the current collector was about 2.2 mg with 1.1 mg of the active materials. After that, the cells (CR 2032) were assembled in an argon-filled glove box (water and oxidant content less than 0.1 ppm), with

the prepared electrodes as the cathode, lithium foil as the anode, the polypropylene microporous membrane (Celgard, 2300) as a separator, and 1M $LiPF_6$ dissolved in ethylene carbonate (EC) and dimethyl carbonate (DMC) (EC/DMC = 1:1 v/v) as the electrolyte, respectively. And the assembled button battery was maintained for 12 h to make the electrolyte fully permeate into the electrode. The charge-discharge measurements were carried out on a LAND CT2001A in the voltage range of 0.01–3.0 V vs. Li/Li^+, using different constant current densities at room temperature. The cyclic voltammetry (CV) tests were completed with CHI 660E electrochemical working station. And the testing was completed in the two-electrode electrochemical cell with the scanning potential range from 0.01 to 3.0 V and a scanning rate of 1 mV/s. Electrochemical impedance spectroscopy (EIS) tests were completed with CHI 660E electrochemical working station. And the testing was completed in the two-electrode electrochemical cell after several cycles, measuring at an open-circuit voltage state of 1 V with the AC signal generated through a 0.005 V of potential perturbation and the measured frequency ranges from 0.01 to 100 Hz.

Results and discussion

Morphology characterization

A schematic illustration for the fabricating procedure of the GO/oPD hybrid hydrogel and GO/PoPD hybrid nanocomposite is shown in Fig. 1. As can be seen, the obtained graphene oxide with the much open porous space benefits the object molecular contained in the matrix. Furthermore, the GO/oPD hybrid hydrogel aggregation is self-assembled by the electrostatic interaction occurred between the carbonyl-contained groups on the surface of GO layers and the amino groups of the intercalated oPD monomers during the hydrothermal reaction process (as shown in Fig. 1). However, the weak interaction, such as hydrogen bonding, π-π interaction, or electrostatic interaction, cannot guarantee the sufficient strength for the obtained GO/oPD hydrogel in fact, which is fragile under external force. As a result, the oxidation polymerization reaction of o-phenylenediamine among the graphene oxide sheets is in situ implemented to produce strong GO/PoPD hybrid nanocomposite with a stable existence of PoPD among the composite.

SEM micrographs for prepared composite were measured. As observed, the obtained pure PoPD exhibits the dispersed rod-like morphology with a diameter of about 0.5–1.0 μm and a length of 5.0–10.0 μm. Furthermore, those obtained rod-like PoPD consists of the secondary structure with a more slender fiber structure (Fig. 2a and 2b), indicating that rod-like PoPD is formed by a gradual self-assembly process. It is considered that the rigid aromatic structure of o-phenylenediamine molecular, the formed trapezoid polymer molecular structure of PoPD, and the intermolecular hydrogen bonds contribute to the formation of the rod-shaped morphology for GO-PoPD. The micrographs of the as-prepared graphene oxide are depicted in Fig. 2c and 2d, in which some graphene oxide sheets tend to wrinkle and curl together to form agglomeration and some show the slightly folded paper-like structure with a few micrometer dimensions. It will provide much porous space for the objective electrode material. For GO/PoPD hybrid composite (Fig. 2e and 2f), the wrinkle agglomerates of GO can still be observed, but the rod-like morphology of PoPD has disappeared in the composite. Alternatively, some aggregated morphologies can be observed among the dispersed GO matrix, which are assigned to the self-polymerization of PoPD outside the GO/PoPD matrix. The disappeared rod-like morphology of PoPD is attributed to the stronger interaction between GO and o-phenylenediamine monomer during the self-assembly process, which significantly impacts the inter-molecular aggregation behavior of the resulted PoPD during the oxidation polymerization process. As a result, it leads to the disappearance of the original rod-like PoPD, and instead, PoPD exists between GO lamellae or disperses among the GO matrix as observed in the SEM images.

Furthermore, the BET analysis and porous properties were also measured by the low-temperature N_2 adsorption/desorption technique, and the adsorption-desorption curves and the pore size distribution for GO, PoPD, and GO/PoPD hybrid composite were characterized, as shown in Fig. 2g and 2f and Table 1, the three samples exhibit the types II and III nitrogen adsorption/desorption isotherm with the type of H3 hysteresis loop (IUPAC classification) at high relative pressure (Fig. 2g), which is typically associated with adsorption for plate-like aggregation, indicative of the much macroporous structure contained in the samples. The BET-specific surface area measured for pure PoPD is only of 43.1 m^2/g, implying of less porous structure contained in the aromatic diamine polymer. For graphene oxide, it exhibits ~ 561 m^2/g of BET surface areas, which is obviously less than its theoretical value (> 2600 m^2/g for a single graphene sheet) [34] likely due to serious reaggregating and overlapping of graphene sheets during the standing process. As PoPD is introduced among GO sheets, the obtained GO/PoPD hybrid composite exhibits a compromise BET surface area of 347 m^2/g and a pore volume of 1.56 cm^3/g which is obviously larger than that of PoPD (0.41 cm^3/g). The pore size distribution is also calculated (Fig. 2h), in which GO, PoPD, and GO/PoPD composites exhibit a wide-aperture distribution with a peak pore diameter at 4.39, 4.43, and 5.79 nm, respectively. It indicates that the introduction of PoPD prevents the reaggregation of GO sheets and increases the surface area and pore volume of GO/PoPD composite, which as electrode materials will provide large contact areas with electrolytes and will then lead to the improved electrochemical performances.

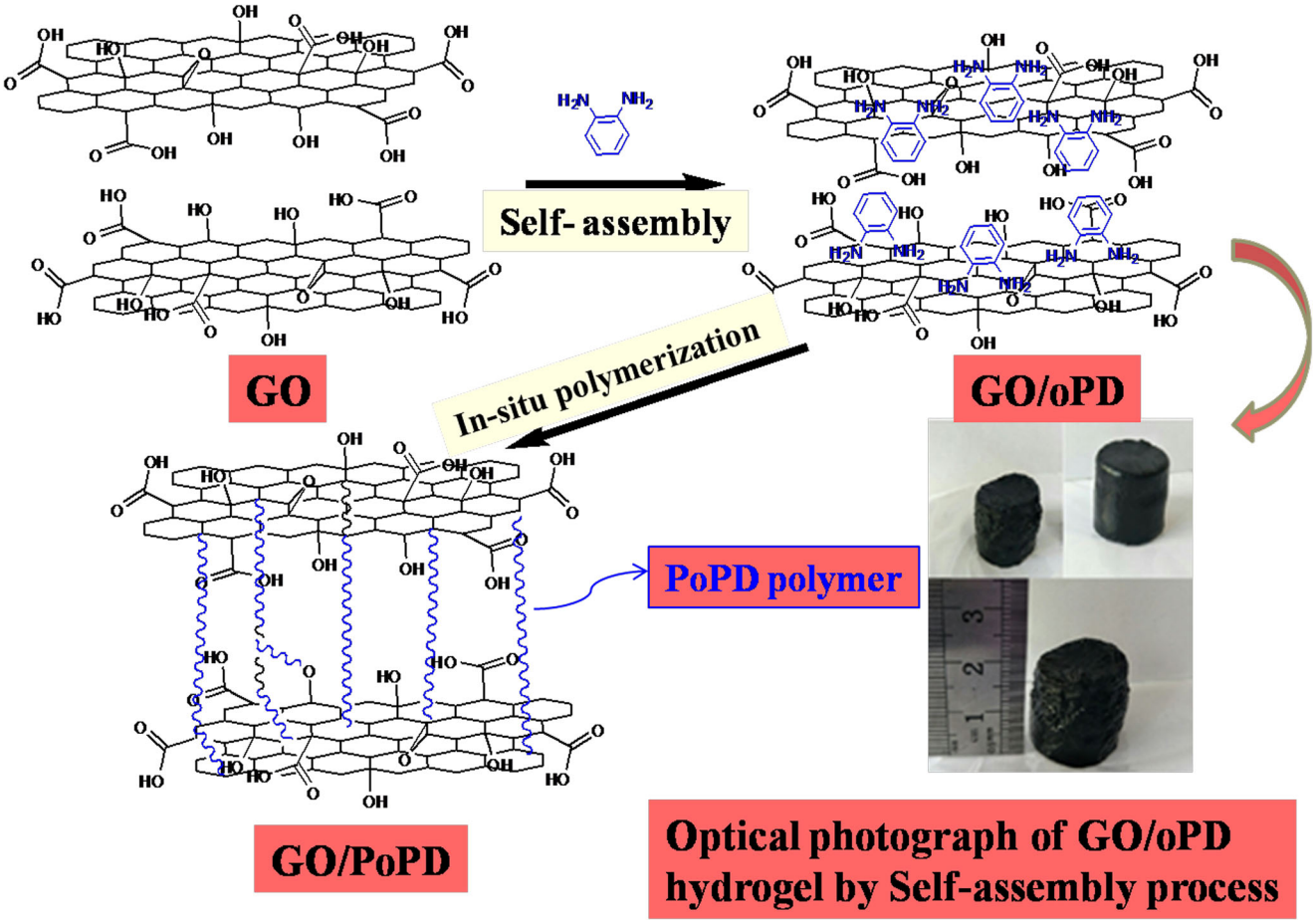

Fig. 1 Schematic illustration of the preparation of GO/oDP hydrid hydrogel and GO/PoPDA hybrid composite

Chemical structure for GO, PoPD, and GO/PoPD hybrid composite was also characterized by FTIR spectra. As shown in Fig. 3, GO presents the series of characteristic absorption bands, centered at ~ 1168 cm^{-1} for the carboxylic groups, at ~ 1727.8 cm^{-1} for the C–O stretching vibrations of the phenolic in the graphene oxides sheets, and at about 1619 cm^{-1} for C=C skeletal vibration of the graphene sheets, respectively [35]. For PoPD, the broad and strong characteristic stretching vibrations at 3345–3129 cm^{-1} implies a large number of imino and amino groups (–NH–/–NH_2) presented in PoPD, while the sharp peak near 1208.7 cm^{-1} corresponds to the C–N stretching vibrational absorption peak of the benzenoid amine structure. Furthermore, it demonstrates that the polymer contains the basic phenazine skeleton, which has been proved by the occurred characteristic peaks at 1635.9 cm^{-1} and 1533.6 cm^{-1} for the C=N and C=C stretching vibrations of phenazine ring and at ~ 837 cm^{-1} for the out-of-plane bending motions of C–H of 1,2,4,5-tetrasubstituted benzene nuclei of phenazine units [36]. However, the observed medium or weak peaks at nearly 752 and 607 cm^{-1} for out-of-plane C–H bending vibration of 1,2,4-trisubstituted benzene nuclei in the phenazine skeleton indicates that the PoPD is not only fully ladder polymers but with a 1,4-substituted benzenoid-quinoid backbone structure contained in the polymer. For the GO/PoPD hybrid composite, the characteristic bands for graphene oxide (C=O (1730 cm^{-1}), C=C (1620 cm^{-1}), C–O–C and C–O (~ 1153 cm^{-1})) and for PoPD (N–H (3171 cm^{-1}) and phenazine (840, 769, 599 cm^{-1})) still appear in the hybrid composite. It strongly demonstrates that both graphene oxide and PoPD are contained in the hybrid composite, and GO/PoPD hybrid composite has been successfully prepared.

Thermal stability was very important for the application of electrode materials in fact, and Fig. 4 showed the TGA curves of GO, PoPD, and GO/PoPD samples. A small weight loss before about 150 °C is related to volatilization of slight water and small molecular which occurred in the samples. With the further temperature-programmed route, an obviously thermal decomposition for PoPD occurs between ~ 320 and 800 °C, in which two thermal degradation platforms with about 82 wt% of the original weight loss are observed in the curve, indicative of two different thermal degradation modes that occurred during the thermal process. According to the molecular structure analysis by FTIR, it is considered as the thermal decomposition of the 1,4-substituted benzenoid-quinoid backbone and the phenazine skeleton structure, correspondingly. For the GO sample, the main thermal degradation occurs at 150~800 °C with about 23 wt% of weight loss, which is

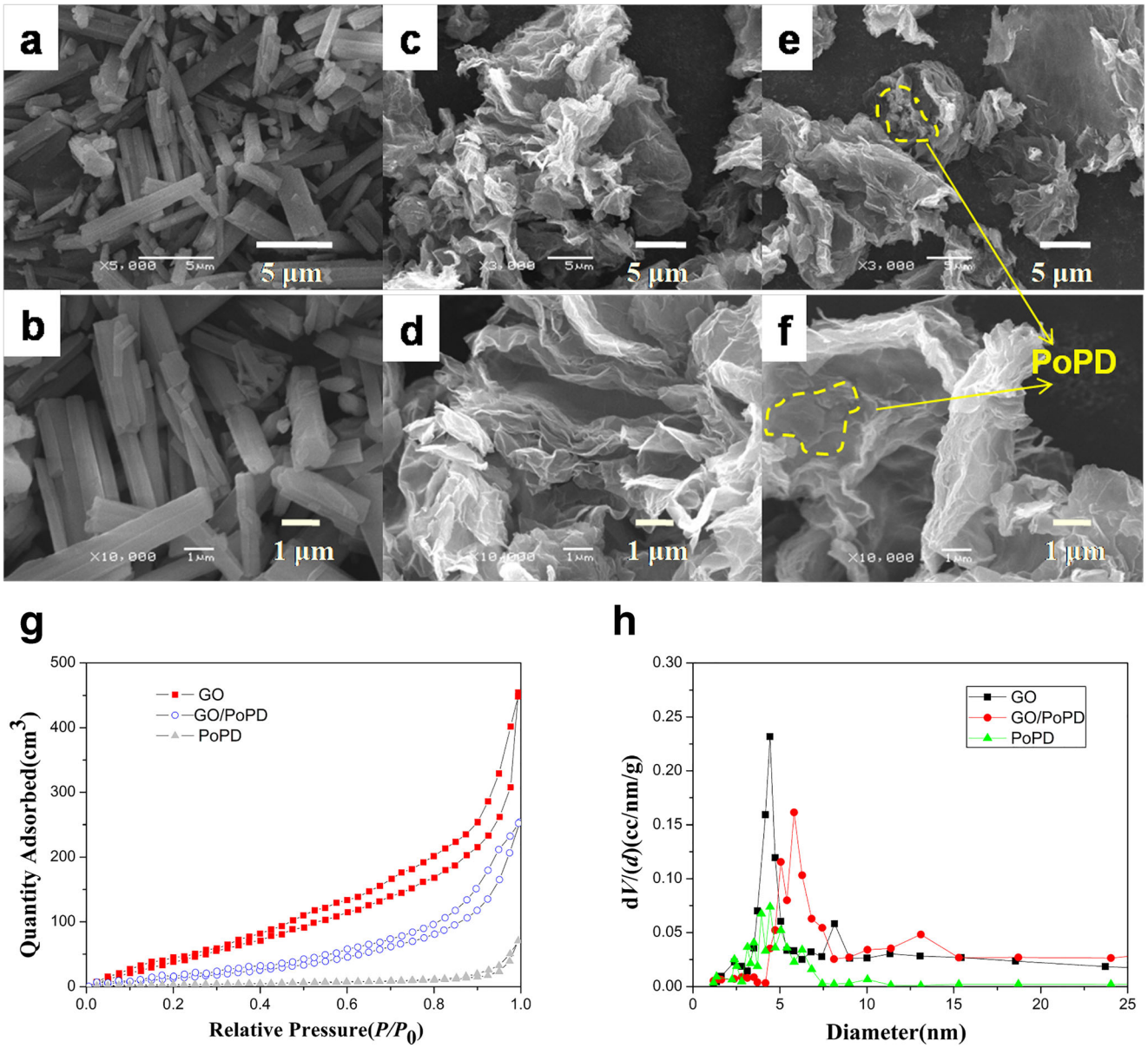

Fig. 2 (a), (b) SEM images of poly(phenylenediamine) (PoPD). (c), (d) SEM images of graphene oxide (GO). (e), (f) SEM images of graphene oxide/poly(phenylenediamine) (GO/PoPD). (g) N_2 adsorption/desorption isotherms of samples. (h) The pore size distribution from the desorption isotherms of samples

related to the thermochemical decomposition of oxygen-contained groups (–OH, –C=O, –COOH, et al.) on the surface of GO. After in situ oxidation polymerization, the obtained GO/PoPD sample demonstrates the comprehensive characteristics of both GO and PoPD with a 34 wt% of weight loss until 800 °C. However, its thermal degradation process is

Table 1 The porous properties of GO/PoPD, GO and PoPD samples

Samples	BET surface areas (m^2/g)	Pore volume (nm)	Peak pore diameter (nm)
GO/PoPD	347	1.56	4.39
GO	561	2.23	5.79
PoPD	43.1	0,41	4.43

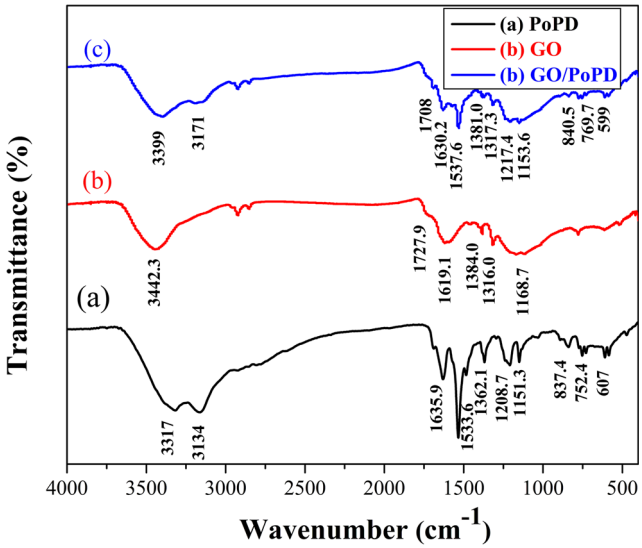

Fig. 3 FTIR spectra of graphene oxide (GO), poly(phenylenediamine) (PoPD), graphene oxide/poly(phenylenediamine) (GO/PoPD)

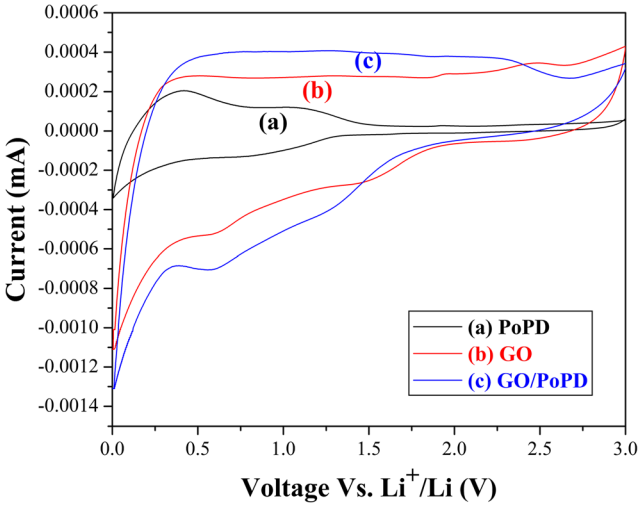

Fig. 5 Cyclic voltammetry of graphene oxide (GO), poly(phenylenediamine) (PoPD), graphene oxide/poly(phenylenediamine) (GO/PoPD) in coin-type cells with the scanning potential range from 0.01 to 3 V and a scanning rate of 1 mV/s

significantly improved compared with that of PoPD, which can be ascribed to the stronger interaction between GO and PoPD.

Electrochemical performances

To investigate the electrochemical behaviors of three samples, the cyclic voltammetry (CV) measurement was initially performed in the voltage range of 0.01–3.0 V at a scan rate of 1 mV/s. Notably, there are some differences among three samples in the CV curves, especially for the lithiation band (Fig. 5). For PoPD, there are two pairs of characteristic peaks during the first scanning, in which the peaks at around 0.9/1.3 V can be attributed to the insertion/deinsertion of lithium ion from nitrogen atoms of PoPD, while a pair of extending broad peaks at the low potential is assigned to the intercalation/deintercalation of lithium ion from C_6 aromatic rings as well as the formation of solid electrolyte interphase (SEI) film on the surface of the lithium electrode. For GO, the first cathodic peaks at ~ 1.4 V is due to the reduction of existed carbonyl groups that occurred on the surface of GO, and the other one at ~ 0.6 V and below corresponds to the insertion of lithium ions into GO as well as the formation of SEI at the anode surface. In comparison, GO/PoPD hybrid composite exhibits the similar redox characteristics but with an even broad redox peak area, implying of the stronger charge storage ability during the electrochemical process.

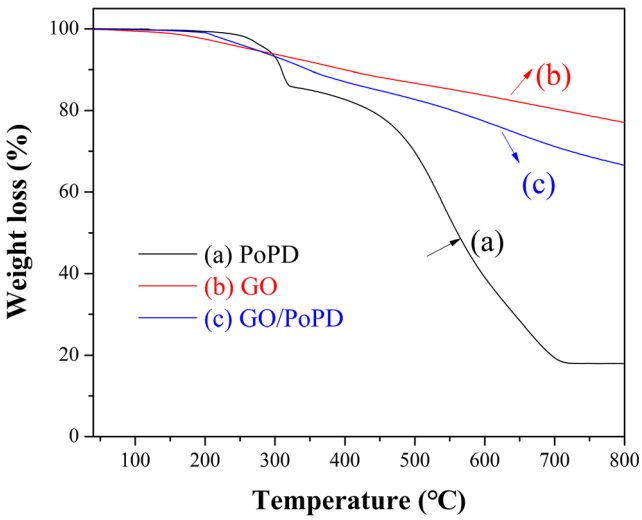

Fig. 4 TGA profiles for the three electrochemical materials of (a) PoPD, (b) GO, and (c) GO/PoPD, running from room temperature to 800 °C at a heating rate of 10 °C/min in air

Cell performances

The charge/discharge performances of GO, PoPD, and GO/PoPD samples as the anode materials were explored with a two-electrode electrochemical cell. Figure 6A exhibits the initial charge/discharge curves of three-electrode materials at the current density of 20 mA/g. The pure PoPD has the charge- and discharge-specific capacities of 803.2 and 1283.4 mAh/g, respectively, and displays an obviously discharge platform in the voltage of ~ 1.7 V, which is attributed to the lithiation of nitrogen atoms in PoPD. For GO, it exhibits an obviously higher capacity of 871 mAh/g than its theory capacity of 740 mAh/g, due to redox contribution from the existing carbonyl groups on the surface of GO, which is characterized by an even discharge platform at the ~ 1.65 V observed in the discharge curve. Comparatively, the GO/PoPD hybrid composite exhibits a remarkably higher charge-specific capacity of 957.4 mAh/g than that of GO but with an almost unchanged discharge-specific capacity of 1632.4 mAh/g. The increased discharge capacity can be attributed to a significant increase of lithium insertion sites among the

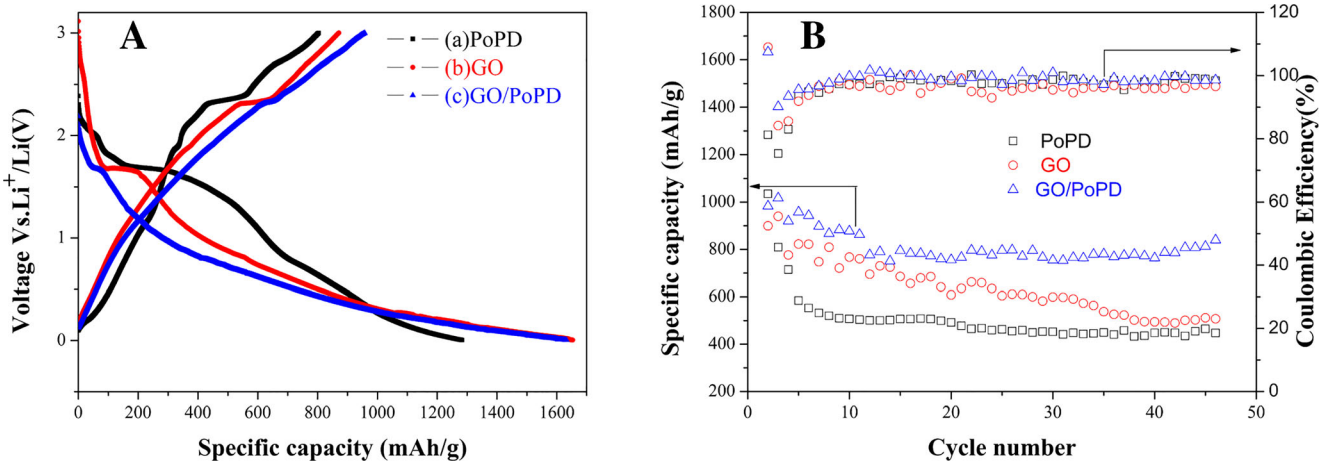

Fig. 6 (A) Initial charge and discharge profiles and (B) cycling stability and coulombic efficiency for the three electrochemical materials: PoPD, GO, and GO/PoPD at a current of 20 mA/g in $LiPF_6$ EC/DMC (v/v, 1:1) electrolyte versus Li/Li^+

GO/PoPD hybrid composite by the introduction of PoPD among GO sheets. Correspondingly, the coulombic efficiency (CE) for GO/PoPD hybrid composite (58.65%) is improved as compared with that of GO (52.86%), due to the enhanced structure stability for GO/PoPD hybrid composites. Also, GO/PoPD hybrid composite still keeps the reaction characteristics of the carbonyl group in the voltage of ~ 1.65 V but with a short discharge platform, due to the decreased quantity of GO in GO/PoPD hybrid composite.

Figure 6B presents the cycling stability of PoPD, GO, and GO/PoPD electrodes in the working potential scope of 0.01–3.0 V, respectively. The results show that the discharge-specific capacity of PoPD in the initial several cycles declines sharply from 1283.4 mAh/g of the first cycle to 586.5 mAh/g of the 4th cycle, and it then keeps relative stability until the 43rd cycle, with the specific capacity of 447.2 mAh/g in the end. The serious capacity decay in the initial several cycles is due to the SEI that occurred by electrolyte decomposition on the surface of a lithium anode, which consumes much of the electrolyte and leads to a serious decrease of capacity at the initial cycles. For GO and GO/POPD, the significant capacity degradation can still be observed in the first few cycles, but it presents different characteristics in the following cycles. For GO, its discharge capacity is unstable and gradually declines with an increasing charge/discharge cycles, due to a gradual loss of unstable lithium insertion sites by the reaggregation process of GO sheets and the irreversible redox process of the presented carbonyl groups on the surface of GO. And there remains only a 507.3 mAh/g of discharge-specific capacity at the 43rd cycle. In contrast, the GO/PoPD electrode presents improved cycling stability, and the discharge capacity after the first few cycles keeps stable even with a slight increase with further cycling. After 43 cycles, it still keeps a capacity of 839.5 mAh/g for GO/PoPD. The improved capacity retention can be attributed to the stable structure formed by the introduced PoPD molecular between GO sheets, which prevents the reaggregation of the graphene sheets. In addition, the stronger interaction between graphene sheets and PoPD by the hydrogen bonds and π-π interaction also benefits to stabilize the GO/PoPD composites, leading to the improved the cyclability of the electrode materials. Furthermore, three samples show the low coulombic efficiency in the initial cycles, due to the side reaction process during the formation of SEI film on the surface of the electrode. And then, the coulombic efficiency for three samples tends to stabilize with its values close to nearly 98–99% for GO/PoPD, 96–98% for PoPD, and only 95–97% for GO, respectively, in which GO/PoPD presents an improved coulombic efficiency as compared with both PoPD and GO, which is consistent with its improved cycling stability.

Figure 7A further presented the rate performances of PoPD, GO, and GO/PoPD electrodes in working potential scopes of 0.01–3.0 V at various current rates of 50, 100, 200, and 500 mA/g, respectively. As shown in the figure, three electrodes display a rapid decrease of capacity in the initial cycles, which are in accord with the cyclability testing. Obviously, the GO/PoPD electrode exhibits a higher capacity than both PoPD and GO electrodes with an enhanced current rate from 50 to 500 mA/g, in which the specific capacity change from 1141.7, 718.2, 621.2 to 567.3 mAh/g for GO/PoPD electrode, 1189.4, 603.1, 457.8 to 359.3 mAh/g for GO electrode, and 983.3, 379.2, 317.3 to 218.8 mAh/g for PoPD electrode, at current rates of 50, 100, 200, and 500 mA/g, respectively (Table 2). The possible reasons for the improved rate performances of GO/PoPD hybrid composite can be ascribed to the enhanced electrical conductivity of the electrode and the constructed stable pore structure by introducing GO presented in the composite, which improves the electron/ion migration among the composite electrode and then results in the decreased polarization as well as the high utilization ratio of active materials during the charge/discharge process. Furthermore, the inherent high capacity of GO/PoPD composite can also contribute to the final high capacity. In addition, the charge-discharge profiles of the as-prepared polymers at different current rates are further presented in Fig. 7B. For PoPD, it

Table 2 Cell performances of GO/PoPD, GO and PoPD samples

Samples	GO/PoPD	GO	PoPD
The initial charge/discharge capacity (mAh/g)	957.4/1632.4	871/1657.1	803.2/1283.4
The initial coulombic efficiency (%)	58.6	52.8	62.6
The reversible capacity after 43 cycles (mAh/g)	839.5	507.3	447.2
The capacity retention (%)	51.4	30.6	34.8
Rate capacity at 50 mA/g (mAh/g)	1411.7	1189.5	983.3
Rate capacity at 100 mA/g (mAh/g)	718.2	603.1	379.2
Rate capacity at 200 mA/g (mAh/g)	621.2	457.8	317.3
Rate capacity at 500 mA/g (mAh/g)	576.3	359.7	218.8

displays the reduced discharge capacity with increasing the discharge rate due to the enhanced polarization, but the discharge curve shape is still kept at different current rates, indicative of a stable redox process, while, for GO and GO/PoPD electrode, the discharge platform at ~ 1.65 V disappears with enhanced discharge current, owning to the gradually decayed redox process from the carbonyl groups during the charge/discharge process. But the shapes of discharge curves, in the following cycling, keep stable even at the current rate of 500 mA/g, implying of the low polarization for the electrode during the charge-discharge process.

Electrochemical impedance spectroscopy (EIS) measurement also confirmed the fast kinetics for charge carrier insertion/extraction from GO/PoPD electrode. As shown in Fig. 8a, all material-based electrodes in Nyquist plots consist of semicircle in the high-frequency region and straight line in the low-frequency region, in which the diameter of the semi-circular can be assigned to the charge transfer impedance (R_{ct}) at the electrode interface, while the straight line in low-frequency region is due to the diffuse control process. From the figure, the charge transfer resistance (R_{ct}) varies with different cathodes: 275 Ω for PoPD, 73 Ω for GO, and only 50 Ω for GO/PoPD, respectively. The small R_{ct} values for GO/PoPD and GO compared with PoPD imply the faster charge transfer within GO/PoPD and GO, which supports the improved electrochemical performance for GO/PoPD during the charge/discharge process. Furthermore, the slope of the straight lines in Nyquist plots becomes more steep for GO/PoPD > GO > PoPD, indicating that the electrode process of GO/PoPD and GO is not only completely diffusion control process but also capacitive behavior process. For the detailed investigation, impedance behavior for GO/PoPD, GO, and PoPD samples was further indicated by Bode absolute and Bode phase diagrams. As shown in Fig. 8b, GO/PoPD and PoPD samples present higher intersect values in both the low- and high-frequency regions than that of GO, indicative of less capacitive behavior. While GO/PoPD exhibits smaller intersect impedance value (Z) than GO and PoPD at the lower frequency, which is consistent with the Nyquist result. Based on the Bode angle diagram, it is observed that the intersect values in the low-frequency region for three electrodes lies between 50o and 70o, which is the characteristic capacitance or adsorption behavior of electrode materials, while the intersect values in the high-frequency region still remain as relatively high values, implying the coexistence of electrical double-layer capacitance and

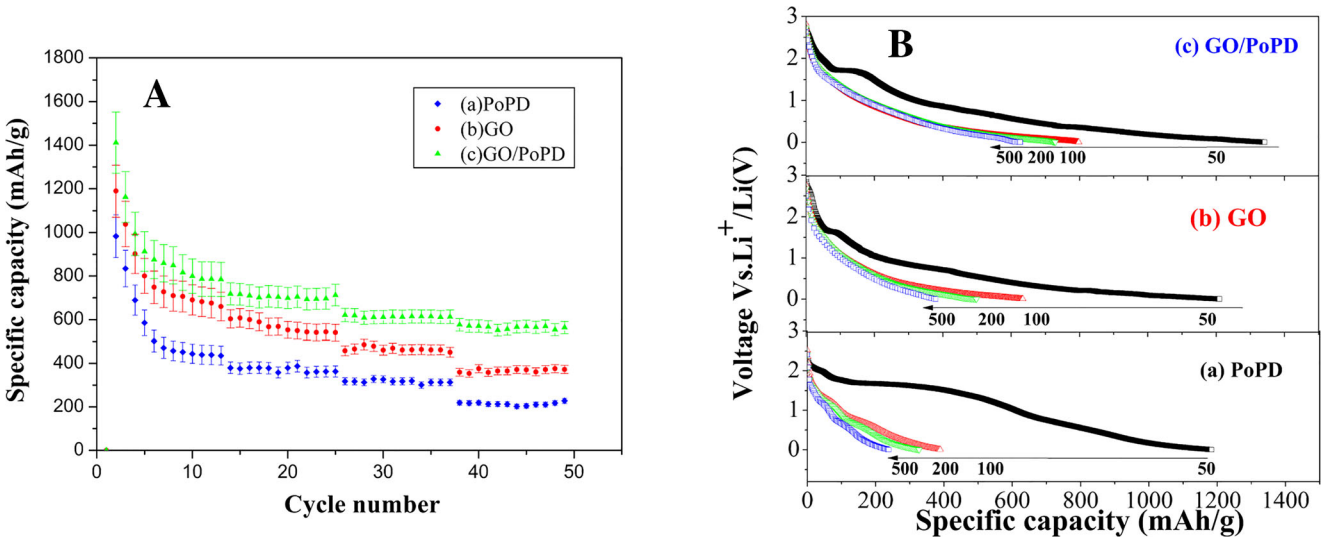

Fig. 7 Rate performances (A) and discharge profile (B) of PoPD, GO, and GO/PoPD electrodes at various current rates of 50, 100, 200, and 500 mA/g, respectively

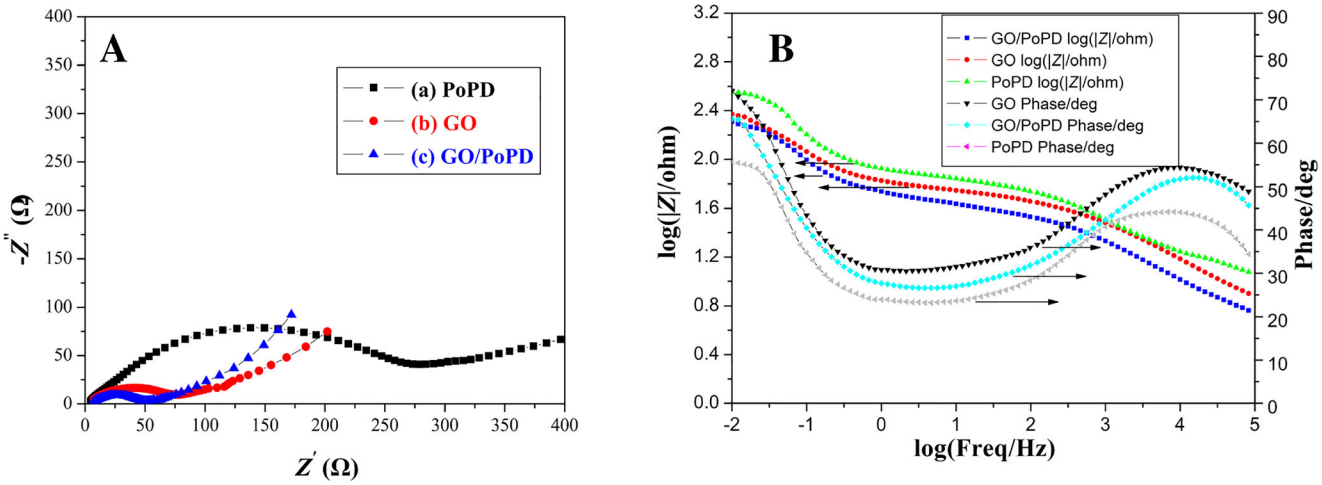

Fig. 8 (a) Nyquist spectra and (b) Bode diagram of PoPD, GO, and GO/PoPD electrodes in the Li/electrolyte/sample configuration

pseudocapacitance. It indicates that the created stable porous morphology and high surface area by introducing PoPD can make it easy for the electrolyte ion to penetrate during the redox reaction, thus leading to the improved cell performances.

Conclusions

In this paper, GO/oPD hydrogel was firstly self-assembled by the hydrothermal method using o-phenylenediamine as an intercalation molecule, and then in situ oxidation polymerization was applied to prepare GO/PoPD hybrid composite. The resulted GO/PoPD hybrid composite possessed an open porous structure, high BET surface area of 347 m^2/g, and improved pore volume of 1.56 cm^3/g. The GO/PoPD hybrid composite as the anode exhibited a high discharge-specific capacity of 1632.4 mAh/g at the first charge/discharge cycle and improved cycling stability as compared with GO. And after 43 cycles, it still kept a capacity of 839.5 mAh/g, which is obviously higher than that of GO and PoPD. Still, the stable coulombic efficiency for GO/PoPD was close to nearly 98–99%, which is consistent with its improved cycling stability. Furthermore, GO/PoPD hybrid composite presented the enhanced rate performances with the discharge-specific capacities of 1411.7, 718.2, 621.2, and 576.3 mAh/g at current rates of 50, 100, 200, and 500 mA/g, respectively. Also, EIS analysis proved that the GO/PoPD hybrid composite has the smallest charge transfer impedance among three samples, which supported its high rate performances.

Funding This research received financial support from the National Science Foundation of China (Grant No.51573099), the Natural Science Foundation of Liaoning Province, China (Grant No.2020-MS-232), the Support Plan for Innovative Talents in Colleges and Universities in Liaoning Province (LR2017034), and the Liaoning BaiQianWan Talents Program.

References

1. Winter BM, Besenhard JO, Spahr ME, Novák P (1998) Insertion electrode materials for rechargeable lithium batteries. Adv Mater 10:725–763
2. Goodenough JB, Kim Y (2010) Challenges for rechargeable Li batteries. Chem Mater 22:587–603
3. Long W, Fang B, Ignaszak A, Wu Z, Wang YJ, Wilkinson D (2015) Nanostructured transition metal oxides as advanced anodes for lithium-ion batteries. Sci Bull 60:823–838
4. Sun WW, Yong W (2014) Graphene-based nanocomposite anodes for lithium-ion batteries. Nanoscale 6:111528–111552
5. Casas de las C, Li WZ (2012) A review of application of carbon nanotubes for lithium ion battery anode material. J Power Sources 208:74–85
6. Hou HS, Qiu XQ, Wei WF, Zhang Y, Ji XB (2017) Carbon anode materials for advanced sodium-ion batteries. Adv Energy Mater 7: 1602898
7. Qi W, Shapter JG, Wu Q, Yin T, Gao G, Cui DX (2017) Nanostructured anode materials for lithium-ion batteries: principle, recent progress and future perspectives. J Mater Chem A 5:19521–19540
8. Zhang SS, Xu K, Jow TR (2004) Electrochemical impedance study on the low temperature of Li-ion batteries. Electrochim Acta 49: 1057–1061
9. Liu Y, Xue JS, Zheng T, Dahn JR (1996) Mechanism of lithium insertion in hard carbons. Carbon 34:193–200
10. Lee KT, Lytle JC, Ergang NS, Oh SM, Stein A (2005) Synthesis and rate performance of monolithic macroporous carbon electrodes for lithium-ion secondary batteries. Adv Funct Mater 15:547–556
11. Guo P, Song H, Chen X (2009) Electrochemical performance of graphene nanosheets as anode material for lithium-ion batteries. Electrochem Commun 11:1320–1324
12. Yoo E, Kim J, Hosono E, Zhou HS, Kudo T, Honma I (2008) Large reversible Li storage of graphene nanosheet families for use in rechargeable lithium ion batteries. Nano Lett 8:2277–2282
13. Liang M, Zhi L (2009) Graphene-based electrode materials for rechargeable lithium batteries. J Mater Chem 19:5871–5878
14. Park S, Ruoff RS (2009) Chemical methods for the production of graphenes. Nat Nanotechnol 4:217–224
15. Cai D, Ding L, Wang S, Li Z, Zhu M, Wang H (2014) Facile synthesis of ultrathin-shell graphene hollow spheres for high-performance lithium-ion batteries. Electrochim Acta 139:96–103

16. Choi BG, Yang M, Hong WH, Choi JW, Huh YS (2012) 3D macroporous graphene frameworks for supercapacitors with high energy and power densities. ACS Nano 6:4020–4028
17. Park SH, Kim HK, Yoon SB, Lee CW, Ahn D, Lee SI, Roh KC, Kim KB (2015) Spray-assisted deep-frying process for the in situ spherical assembly of graphene for energy-storage devices. Chem Mater 27:457–465
18. Fan Z, Yan J, Ning G, Wei T, Zhi L, Wei F (2013) Porous graphene networks as high performance anode materials for lithium ion batteries. Carbon 60:558–561
19. Vickery JL, Patil AJ, Mann S (2009) Fabrication of graphene–polymer nanocomposites with higher-order three-dimensional architectures. Adv Mater 21:2180–2184
20. Yang S, Feng X, Zhi L, Cao Q, Maier J, Müllen K (2010) Nanographene-constructed hollow carbon spheres and their favorable electroactivity with respect to lithium storage. Adv Mater 22: 838–842
21. Yin S, Zhang Y, Kong J, Zou C, Li CM, Lu X, Ma J, Boey FYC, Chen X (2011) Assembly of graphene sheets into hierarchical structures for high-performance energy storage. ACS Nano 5:3831–3838
22. Fang Q, Shen Y, Chen B (2015) Synthesis, decoration and properties of three-dimensional graphene-based macrostructures: a review. Chem Eng J 264:753–771
23. Bai H, Li C, Wang X, Shi G (2011) On the gelation of graphene oxide. J Phys Chem C 115:5545–5551
24. Tung VC, Kim J, Cote LJ, Huang J (2011) Sticky interconnect for solution-processed tandem Solar cells. J Am Chem Soc 133:9262–9265
25. Xu Y, Wu Q, Sun Y, Bai H, Shi G (2010) Three-dimensional self-assembly of graphene oxide and DNA into multifunctional hydrogels. ACS Nano 4:7358–7362
26. Adhikari B, Biswas A, Banerjee A (2012) Graphene oxide-based supramolecular hydrogels for making nanohybrid systems with Au nanoparticles. Langmuir 28:1460–1469
27. Jiang X, Ma Y, Li J, Fan Q, Huang W (2010) Self-Assembly of reduced graphene oxide into three-dimensional architecture by divalent ion linkage. J Phys Chem C 114:22462–22465
28. Chang YZ, Han GY, Yuan JP, Fu DY, Liu FF, Li SD (2013) Using hydroxylamine as a reducer to prepare N-doped graphene hydrogels used in high-performance energy storag. J Power Sources 238:492–500
29. Yang C, Hu NT, Wang WY, Cao BQ (2018) Surface-crumpled graphene hydrogels with macro- and microporous structures for ultrahigh-volumetric energy storage. J Power Sources 399:115–124
30. Oyama N, Ohsaka T (1987) Electrochemical properties of the polymer films prepared by electrochemical polymerization of aromatic compounds with amino groups. Synth Met 18:375–380
31. Zhang K, Zhang LL, Zhao XS, Wu J (2010) Graphene/polyaniline nanofiber composites as supercapacitor electrodes. Chem Mater 22: 1392–1401
32. Chen J, Liu Y, Minett AI, Lynam C, Wang J, Wallace GG (2007) Flexible, aligned carbon nanotube/conducting polymer electrodes for a lithium-ion battery. Chem Mater 19:3595–3597
33. Hummers WS, Offeman RE (1958) Preparation of graphitic oxide. J Am Chem Soc 80:1339–1339
34. Peigney A, Laurent C, Flahaut E, Bacsa RR, Rousset A (2001) Specific surface area of carbon nanotubes and bundles of carbon nanotubes. Carbon 39:507–514
35. Li R, Chen CB, Li J, Xu LM, Xiao GY, Yan DY (2014) A facile approach to superhydrophobic and superoleophilic graphene/polymer aerogels. J Mater Chem A 2:3057–3064
36. Yano J (1995) Electrochemical and structural studies on soluble and conducting polymer fromo-phenylenediamine. J Polym Sci A Polym Chem 33:2435–2441